Defect and Diffusion Forum
ISSN: 1662-9507, Vol. 409, pp 17-38
doi:10.4028/www.scientific.net/DDF.409.17

Submitted: 2020-07-25
Revised: 2021-01-30
Accepted: 2021-01-30
Online: 2021-05-18

Time-Dependent Hydromagnetic Boundary Layer Flow Across a Porous Vertical Surface with Internal Heat Generation

Musah Sulemana[1], Ibrahim Yakubu Seini[2*]

[1]Faculty of Mathematical Sciences, University for Development Studies, P. O. Box 1350, Tamale

[2]School of Engineering, University for Development Studies, P. O. Box 1350, Tamale

[a]wunichee@yahoo.com, [b]dr.yseini@uds.edu.gh

*Corresponding author

Keywords: unsteady flow; magnetic field; incompressible fluid; porous medium; Laplace transform

Abstract. The time-dependent hydromagnetic boundary layer flow across a vertical surface with internal heat regeneration in porous media is investigated. The flow problem has been modelled mathematically in partial differential equations along with appropriate defined boundary conditions. These equations were expressed in dimensionless form using suitable similarity variables. The resulting dimensionless equations along with the conditions defined at the boundaries are solved by means of the Laplace transform methods. Results of the study are graphically illustrated for various quantities of practical importance. It was concluded that time positively influence the flow as a reduced skin friction coefficient was observed. Furthermore, the magnetic parameter, the radiation parameter, the heat absorption parameter and the permeability of the porous media can be used to influence the characteristics of a flow in porous media.

Introduction

Heat transfer is said to occur when there exist temperature differences between two bodies. When there exists temperature difference between two bodies, heat tends to move from the body with higher temperature to the lower temperature body. Heat and mass transfer processes are time-dependent and are generally referred to as unsteady processes. Research into unsteady processes has led to improvements in industrial practices and performance of systems. It is encountered in the design of streamlined objects such as helicopter blades, turbine blades, compressors and start-up processes involving periodic fluid motion as well as in the area of convective heat and mass transfers [1]. Other areas of relevance include petroleum exploration, thermal oil recovery, geophysics and astrophysics. Unsteady processes are encountered in industrial and environmental processes. It occurs during the evaporation of open water reservoirs to cooling and heating processes and in the combustion of fossil fuels. Many researchers have used different methods to study the unsteady flow problem. The perturbation method [2] has been used to investigate various convection flow processes with viscous dissipation [3], Newtonian heating [4], and accelerated vertical surfaces [5]. Other used the Laplace transform techniques to investigate the free unsteady convective flow across surface with impulsive starting in Newtonian fluid media [6]. The permeability and radiation of MHD flow in a uniform heat flux [7] contribute to heat dissipation. Radiation from isothermally accelerated vertical surface with internal heating and chemical reaction [8] reveals a direct correlation between the Grashof number, Gr and the velocity of flow. With variable temperature [9], the fluid temperature increased with the radiation.

The hydromagnetic boundary layer flow due to exponential stretching surface, radiation and chemical reaction has been extensively reported [10-13] with observations that the rate of heat transfer at the surface diminishes with high parameter values of magnetic field strength and radiation. A reduction in the velocity profiles due to increasing magnetic field strength, Prandtl number and Eckert number has been observed [14] with the reverse for increasing Grashof numbers.

The Newton Raphson shooting method [15] along with the Fourth-Order Runge - Kutta algorithm [16] has been used to investigate the free unsteady hydromagnetic boundary layer problem. The Laplace transform techniques has also been used to analyse the unsteady flow of Casson fluid near a

vertical oscillating surface under the influence of Newtonian heating [17] and observed that the velocity of flow diminished with the Casson parameter. However, the thickness of the thermal boundary enlarged with increasing Newtonian heating. The technique has also been used to analyse the effects of the Soret number [18] on the mixed convective flow with heat and mass transfer in porous media [19, 20].

This study incorporates the nonlinear velocity term in the energy equation due to its practical relevance in many industrial applications. The Laplace transform technique is used in this study due to its robustness in solving highly nonlinear problems.

Problem Formulation

Consider a time-dependent magnetohydrodynamic boundary layer flow across surface vertically aligned in a porous medium undergoing internal heat generation. Assuming a negligible induced magnetic field with a small Reynolds number and a negligible viscous dissipation. Assuming that the flow is in the direction of $x^* - axis$ directed along the vertical plate in the upward direction. Taking the y^* −axis as normal to the surface, with the temperature of the plate and the ambient fluid being $T_w^*(x)$ and T_∞^* respectively.

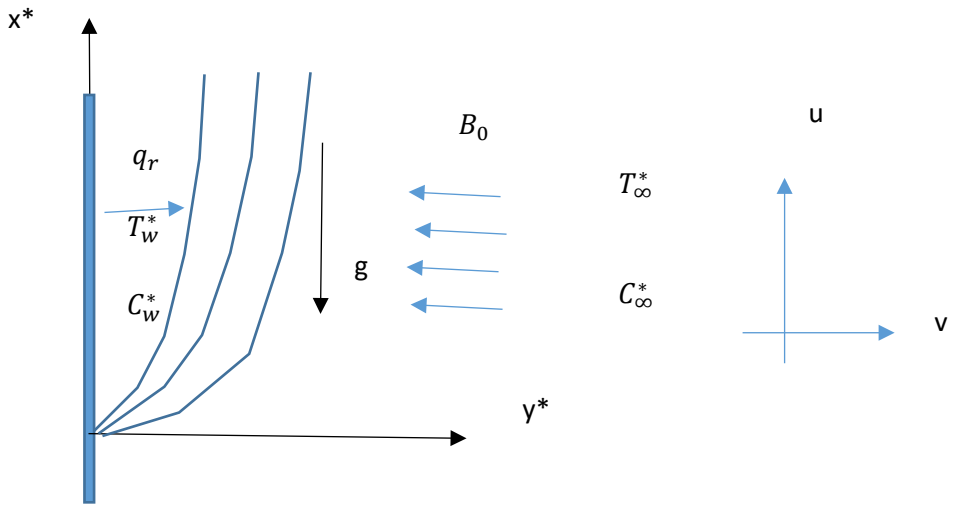

Fig. 1: Flow Configuration.

Furthermore, assuming that the plate and the fluid are in thermal equilibrium with temperature T_∞^* and concentration level C_∞^* at all points. At time $t^* > 0$, the plate is assumed to accelerate exponentially with velocity $u = U_0 e^{a^* t^*}$ in its own plane with the temperature raised linearly whilst the concentration levels near the surface is raised to C_w^*. Assuming the fluid is a gray gas, which absorbs or emits heat. The physical properties of the fluid such as the viscosity and thermal conductivity are assumed constant, while *Boussinesq* approximation is invoked for the density variation in the body force term of the momentum equation. Under these assumptions, the governing equations of the process are:

$$\frac{\partial v^*}{\partial y^*} = 0. \tag{1}$$

$$\frac{\partial u^*}{\partial t^*} = \nu \frac{\partial^2 u^*}{\partial y^{*2}} + g\beta_T (T^* - T_\infty^*) + g\beta_C (C^* - C^*_\infty) - \frac{\sigma B_0^2}{\rho} u^* - \frac{\nu}{k^*} u^*. \tag{2}$$

$$\frac{\partial T^*}{\partial t^*} = \alpha \frac{\partial^2 T^*}{\partial y^{*2}} - \frac{1}{\rho c_p} \frac{\partial q_r}{\partial y^*} - \frac{Q}{\rho c_p} (T^* - T^*_\infty) + \frac{\sigma B_0^{\,2}}{\rho c_p} u^{*2}. \tag{3}$$

$$\frac{\partial C^*}{\partial t^*} = D \frac{\partial^2 C^*}{\partial y^{*2}} - K_C^{\,*} (C^* - C^*_\infty). \tag{4}$$

With boundary conditions

$$u^* = 0,\ T^* = T_\infty^* \qquad C^* = C_\infty^*\ for\ all\ y^*,\ t^* \le 0;$$
$$u^* = U_0 e^{a*t*}, T^* = T_\infty^* + (T_w^* - T_\infty^*)At^*,\ C^* = C_w^*\ at\ y^* = 0,\ t^* > 0;$$
$$u^* \to 0,\ T^* \to T_\infty^*,\ C^* \to C_\infty^*\ as\ y^* \to \infty,\ t^* > 0. \tag{5}$$

where u^* and v^* are the horizontal and vertical velocity components; U_0 denotes the velocity of the plate; y^* denotes the coordinate axis normal to the surface; t^* is time; v is kinematic viscosity; β_T is thermal expansion coefficient; β_C is concentration expansion co-efficient; ρ is fluid density; T^* is the fluid temperature near the surface; T_w^* is the fluid temperature at the surface; T_∞^* is the temperature of the free stream; C^* is the concentration in the fluid; C_∞^* is the concentration far away from the surface; C_w^* is the concentration at the surface; a is the acceleration parameter; D is the chemical molecular diffusivity; $\propto$ is thermal diffusivity; c_p is specific heat at constant pressure; K_c^* is rate of chemical reaction; k* is permeability co-efficient of the porous medium, q_r is the radiation heat flux, Q is the heat source parameter.

The following dimensionless variables and parameters as used in [8] are introduced:

$$u = \frac{u*}{U_0},\quad y = \frac{U_0 y*}{v},\quad Q = \frac{vQ_0}{U_0^2 \rho C_p},\quad \theta = \frac{T^* - T_\infty^*}{T_w^* - T_\infty^*},\ t = \frac{t^* U_0^2}{v},\quad k = \frac{U_0^2 k^*}{v^2},\ \phi = \frac{C^* - C_\infty^*}{C_w^* - C_\infty},$$
$$P_r = \frac{\mu C_p}{k} = \frac{v}{\propto},\quad M = \frac{\sigma B_0^2 v}{\rho U_0^2},\ Gr = \frac{v\, g\beta_T (T_w^* - T_\infty^*)}{U_0^3},\ Gc = \frac{v\, g\beta_C (C_w^* - C_\infty^*)}{U_0^3},\ k_c = \frac{v\, k_c^*}{U_0^2},\ H = \frac{Qv^2}{kU_0^2},$$
$$a = \frac{a^* v}{U_0^2},\ A = \frac{U_0^2}{v},\quad F = \frac{16\sigma a^* v^2 T_\infty^{*3}}{KU_0^2},\ Ec = \frac{u^2}{C_p (T_w^* - T_\infty^*)}. \tag{6}$$

where y is a dimensionless coordinate axis normal to the surface; u is the dimensionless velocity in the x direction; θ is the dimensionless temperature; t is dimensionless time; k is dimensionless permeability of the porous medium; F is the radiation parameter; M is the magnetic parameter; H is the heat absorption parameter; A is a constant; B_0 is the uniform external magnetic field; μ is the dynamic viscosity**;** Sc is the Schmidt number; Pr is the Prandtl number; Gr is the thermal Grashof number; Gc is the solutal Grashof number; Q is the heat source parameter; σ is the electrical conductivity; ϕ is the dimensionless concentration in the fluid; g is the acceleration due to gravity; K is the thermal conductivity of the fluid; K_C is dimensionless rate of chemical reaction; Ec is the Eckert number.

Using the Rosseland approximation;

$$\frac{\partial q_r}{\partial y^*} = -4a^*\sigma^*(T_\infty^{*4} - T^{*4}). \tag{7}$$

where $a^* =$ Rosseland mean absorption co-efficient, $\sigma^* =$Stefan-Boltzmann constant and $q_r =$ radiative heat flux.

Assuming that the temperature difference within the flow are sufficiently small such that T^{*4} is expressed as a linear function of the temperature. By Taylor's series expansion and neglecting the higher order terms, T^{*4} is expressed as a linear function of the temperature in the form;

$$T^{*4} \approx 4T_\infty^{*3} T^* - 3T_\infty^{*4}. \tag{8}$$

Substituting equation (8) into equation (7) gives;

$$\frac{\partial q_r}{\partial y^*} = -16a^*\sigma T_\infty^{*3}(T_\infty^* - T^*). \tag{9}$$

Using equations (6) and (9), equations (2) to (4) are reduced to:

$$\frac{\partial u}{\partial t} = \frac{\partial^2 u}{\partial y^2} + Gr\theta + Gc\phi - M_1 u. \tag{10}$$

where $M_1 = M + \frac{1}{K}$.

$$\frac{\partial\theta}{\partial t} = \frac{1}{Pr}\frac{\partial^2\theta}{\partial y^2} - \frac{1}{Pr}F_1\theta + MEcu^2. \quad (11)$$

where $F_1 = F + H$.

$$\frac{\partial\phi}{\partial t} = \frac{1}{Sc}\frac{\partial^2\phi}{\partial y^2} - Kc\phi. \quad (12)$$

With boundary conditions;

$$\begin{aligned} u = 0, \quad \theta = 0, \quad \emptyset = 0 \ \ for\ all\ y, \quad t \le 0; \\ u = e^{at}, \quad \theta = 1, \quad \emptyset = 1 \ \ at \ \ y = 0, \quad t > 0; \\ u \to 0, \quad \theta \to 0, \quad \emptyset \to 0 \ \ as \ \ y \to \infty, \ \ t > 0. \end{aligned} \quad (13)$$

Analytical Solution

The non-linear partial differential equations (10) to (12) along with the boundary conditions (13) are solved exactly using the Laplace transform techniques. These equations are transformed as follow:

From equation (11); $\frac{\partial\theta}{\partial t} = \frac{1}{Pr}\frac{\partial^2\theta}{\partial y^2} - \frac{1}{Pr}F_1\theta + MEcu^2.$

Re-arranging $\frac{1}{Pr}\frac{\partial^2\theta}{\partial y^2} = \frac{\partial\theta}{\partial t} + \frac{1}{Pr}F_1\theta - MEcu^2.$

Taking the Laplace transform of both sides;

$$\frac{1}{Pr}\mathcal{L}[\frac{\partial^2\theta}{\partial y^2}] = \mathcal{L}[\frac{\partial\theta}{\partial t}] + \frac{1}{Pr}F_1\mathcal{L}[\theta] - MEc\mathcal{L}[u^2].$$

Using the Laplace transforms of derivatives from tables;

$$\frac{1}{P_r}\frac{\partial^2\bar{\theta}}{\partial y^2} - s\bar{\theta}(y,s) + \theta(y,0) = \frac{F_1}{P_r}\bar{\theta}(y,s) - MEc\mathcal{L}[u^2] \quad (14)$$

where s is a Laplace transform parameter.
$u \neq$ constant, since u is a function of space and time. i.e. $u(y,t)$.
The boundary condition in Laplace domain as:

$$\begin{aligned} &\theta(y,0) = 0 \ \ for\ all \ \ y \ge 0, \ t \le 0, \quad \bar{\theta}(y,0) = 0; \\ &\theta(0,t) = 1 \quad at \ \ y = 0, \ \ t > 0, \ \bar{\theta}(0,s) = \frac{1}{s}; \\ &\theta(y,t) \to 0 \quad as \quad y \to \infty, \quad t > 0. \quad \bar{\theta}(y,s) \to 0. \end{aligned} \quad (15)$$

The solution to the LHS of equation (14) is expressed as;

$$\bar{\theta}_h(y,s) = A(s)e^{-y\sqrt{P_rs+F_1}} + B(s)e^{y\sqrt{P_rs+F_1}}. \quad (16)$$

Adding the particular solution of the $\frac{P_rMEc}{P_rs+F_1}\mathcal{L}[u^2(y,t)]$ to equation (16) gives the general solution as;

$$\bar{\theta}(y,s) = A(s)e^{-y\sqrt{P_rs+F_1}} + B(s)e^{y\sqrt{P_rs+F_1}} + \frac{P_rMEc}{P_rs+F_1}\mathcal{L}[u^2(y,t)]. \quad (17)$$

Since $\theta(y,t) \to 0 \ as \ \ y \to \infty, \ \ t > 0 \Longrightarrow \theta(y,s) = 0$ and $B(s) = 0$
Equation (17) then reduces to;

$$\bar{\theta}(y,s) = A(s)e^{-y\sqrt{Prs+F_1}} + \frac{PrMEc}{Prs+F_1}\mathcal{L}[u^2(y,t)]. \quad (18)$$

$$\theta(0,t) = 1 \ \ at \ \ y = 0, t > 0 \qquad \Longrightarrow \bar{\theta}(0,s) = \frac{1}{s}$$

From equation (18), $\frac{1}{s} = A(s) + \frac{P_rMEc}{Prs+F_1}\mathcal{L}[u^2(y,t)]$,

Thus, $\bar{\theta}(y,s)=\left(\frac{1}{s}-\frac{PrME_c}{Prs+F_1}\mathcal{L}[u^2(y,t)]\right)e^{-\sqrt{Prs+F_1}\,y}+\frac{PrME_c}{Prs+F_1}L[u^2(y,t)]$

$$\bar{\theta}(y,s)=\frac{1}{s}e^{-\sqrt{Prs+F_1}\,y}+L[u^2(y,t)]PrMEc\left(\frac{1}{Prs+F_1}-\frac{1}{Prs+F_1}e^{-\sqrt{Prs+F_1}\,y}\right). \quad (19)$$

Equation (19) is the general solution of the temperature model in Laplace domain whose inverse will be determined later when the velocity function $u^2(y,t)$ is known.
The dimensionless concentration equation (12) is

$$\frac{\partial\phi}{\partial t}=\frac{1}{Sc}\frac{\partial^2\phi}{\partial y^2}-Kc\phi\,.$$

In Laplace domain, boundary conditions are:

$$\begin{aligned}&\phi(y,0)=0 \quad for\ all \quad y\geq 0, \quad t\leq 0 \qquad \bar{\phi}(y,0)=0;\\ &\phi(0,t)=1\ at \quad y=0, t>0 \qquad\qquad \bar{\phi}(0,s)=\frac{1}{s};\\ &\phi(y,t)\to 0 \quad as \quad y\to\infty, \quad t>0, \quad \bar{\phi}(y,s)\to 0.\end{aligned} \quad (20)$$

The Laplace transform of each term in equation (12) gives;

$$\frac{1}{Sc}\frac{\partial^2\bar{\phi}}{\partial y^2}-s\bar{\phi}(y,s)+\phi(y,0)=K_c\bar{\phi}, \quad (21)$$

Since $\phi(y,0)=0$,

$$\frac{\partial^2\bar{\phi}}{\partial y^2}-Sc(s+K_c)\bar{\phi}=0. \quad (22)$$

Equation (22) is a homogenous linear second order ode whose solution is in the form;

$$\bar{\phi}(y,s)=A(s)e^{-y\sqrt{Scs+ScK_c}}+B(s)e^{y\sqrt{Scs+ScK_c}}. \quad (23)$$

Since, $\phi(y,t)\to 0\ as \quad y\to\infty, \ t>0 \qquad \bar{\phi}(y,s)=0$ and $B(s)=0$

Then equation (23) reduces to;

$$\bar{\phi}(y,s)=A(s)e^{-y\sqrt{Scs+ScK_c}}. \quad (24)$$

But $\phi(0,t)=1 \ at \quad y=0, \quad t>0 \qquad \bar{\phi}(0,s)=\frac{1}{s}$,

From equation (24), $\frac{1}{s}=A(s)$

$$\bar{\phi}(y,s)=\frac{1}{s}e^{-\sqrt{Scs+ScK_c}\,y}. \quad (25)$$

The standard inverse Laplace transform of (25) using convolution theorem is

$$\phi(y,t)=\frac{1}{2}\left[e^{-y\sqrt{ScK_c}}erfc\left(\frac{2t\sqrt{K_c}-y\sqrt{Sc}}{2\sqrt{t}}\right)+e^{y\sqrt{ScK_c}}erfc\left(\frac{2t\sqrt{K_c}+y\sqrt{Sc}}{2\sqrt{t}}\right)\right] \quad (26)$$

Equation (26) is the general solution representing the chemical concentration profile at $t>0$.
Similarly, from the dimensionless momentum equation given in (10) as;

$$\frac{\partial u}{\partial t}=\frac{\partial^2 u}{\partial y^2}+Gr\theta+Gc\phi-M_1u,$$

Subject to the boundary conditions in Laplace domain as:

$$\begin{aligned}&u(y,0)=0 \quad for\ all \quad y\geq 0, \ t\leq 0 \qquad \bar{u}(y,0)=0;\\ &u(0,t)=e^{at}\ at \quad y=0, \ t>0 \qquad\qquad \bar{u}(0,s)=\frac{1}{s-a};\\ &u(y,t)\to 0\ as \quad y\to\infty, \ t>0 \ \ \bar{u}(y,s)\to 0.\end{aligned} \quad (27)$$

The Laplace transform of (10) results in;

$$\frac{\partial^2 \bar{u}}{\partial y^2} - (s+M_1)\bar{u} = -Gr\bar{\theta} - Gc\bar{\phi} \tag{28}$$

The general solution of equation (28) is;

$$\bar{u}(y,s) = \left(\frac{1}{s-a} - \frac{Gr}{s+M_1}\bar{\theta} - \frac{Gc}{s+M_1}\bar{\phi}\right)e^{-y\sqrt{s+M_1}} + \frac{Gr}{s+M_1}\bar{\theta} + \frac{Gc}{s+M_1}\bar{\phi},$$
$$\bar{u}(y,s) = \frac{1}{s-a}e^{-y\sqrt{s+M_1}} + Gr\bar{\theta}\left(\frac{1}{s+M_1} - \frac{1}{s+M_1}e^{-y\sqrt{s+M_1}}\right) + Gc\bar{\phi}\left(\frac{1}{s+M_1} - \frac{1}{s+M_1}e^{-y\sqrt{s+M_1}}\right). \tag{29}$$

The inverse Laplace transform (29) using the convolution theorem gives the general solution as;

$$u(y,t) = -\frac{1}{2}e^{at-y\sqrt{a+M_1}}erfc\left(\frac{2t\sqrt{a+M_1}-y}{2\sqrt{t}}\right) + \frac{1}{2}e^{at+y\sqrt{a+M_1}}erfc\left(\frac{2t\sqrt{a+M_1}+y}{2\sqrt{t}}\right) +$$
$$\left(Gr\theta(y,t) + Gc\phi(y,t)\right)\left(e^{-M_1 t} - e^{-M_1 t}erfc\left(\frac{y}{2\sqrt{t}}\right)\right). \tag{30}$$

Equation (30) is the general solution for the velocity profile at $t > 0$.
The general solution of the temperature model is then obtained as;

$$\theta(y,t) = \frac{1}{2}\left[-e^{-y\sqrt{F_1}}erfc\left(\frac{2t\sqrt{\frac{F_1}{Pr}}-y\sqrt{Pr}}{2\sqrt{t}}\right) + e^{y\sqrt{F_1}}erfc\left(\frac{2t\sqrt{\frac{F_1}{Pr}}+y\sqrt{Pr}}{2\sqrt{t}}\right)\right] +$$
$$u^2(y,t)MEc\left(e^{-\frac{F_1}{Pr}t} - e^{-\frac{F_1}{Pr}t}erfc\left(\frac{y\sqrt{P_r}}{2\sqrt{t}}\right)\right). \tag{31}$$

On substituting $u^2(y,t)$ into equation (31), the non-linear term $\theta^2(y,t)$ is considered negligible since the temperature difference in the flow is sufficiently small. Hence the general solution of the temperature model at $t > 0$ is;

$$\theta(y,t) = \left[1 - MEce^{-\frac{F_1}{P_r}t}\left(1 - erfc\left(\frac{y\sqrt{P_r}}{2\sqrt{t}}\right)\right)\left[2GrGc\phi(y,t)e^{-2M_1 t}\left(1 - 2erfc\left(\frac{y}{2\sqrt{t}}\right) + \left(erfc\left(\frac{y}{2\sqrt{t}}\right)\right)^2\right) + Gr\left(e^{-M_1 t} - e^{-M_1 t}erfc\left(\frac{y}{2\sqrt{t}}\right)\right)\left(-e^{at-y\sqrt{a+M_1}}erfc\left(\frac{2t\sqrt{a+M_1}-y}{2\sqrt{t}}\right) + e^{at+y\sqrt{a+M_1}}erfc\left(\frac{2t\sqrt{a+M_1}+y}{2\sqrt{t}}\right)\right)\right]\right]^{-1}\left[-\frac{1}{2}e^{-y\sqrt{F_1}}erfc\left(\frac{2t\sqrt{\frac{F_1}{Pr}}-y\sqrt{P_r}}{2\sqrt{t}}\right) + \frac{1}{2}e^{y\sqrt{F_1}}erfc\left(\frac{2t\sqrt{\frac{F_1}{Pr}}+y\sqrt{P_r}}{2\sqrt{t}}\right) + MEce^{-\frac{F_1}{P_r}t}\left(1 - erfc\left(\frac{y\sqrt{P_r}}{2\sqrt{t}}\right)\right)\left[\frac{1}{4}e^{2(at-y\sqrt{a+M_1})}\left(erfc\left(\frac{2t\sqrt{a+M_1}-y}{2\sqrt{t}}\right)\right)^2 + \frac{1}{4}e^{2(at+y\sqrt{a+M_1})}\left(erfc\left(\frac{2t\sqrt{a+M_1}+y}{2\sqrt{t}}\right)\right)^2 + G_c^2\phi^2(y,t)e^{-2M_1 t}\left(1 - 2erfc\left(\frac{y}{2\sqrt{t}}\right) + \left(erfc\left(\frac{y}{2\sqrt{t}}\right)\right)^2\right) - \frac{1}{2}e^{2at}erfc\left(\frac{2t\sqrt{a+M_1}-y}{2\sqrt{t}}\right)erfc\left(\frac{2t\sqrt{a+M_1}+y}{2\sqrt{t}}\right) +$$

$$Gc\phi(y,t)\left(e^{-M_1 t}-e^{-M_1 t}erfc\left(\frac{y}{2\sqrt{t}}\right)\right)\left(-e^{at-y\sqrt{a+M_1}}erfc\left(\frac{2t\sqrt{a+M_1}-y}{2\sqrt{t}}\right)+ e^{at+y\sqrt{a+M_1}}erfc\left(\frac{2t\sqrt{a+M_1}+y}{2\sqrt{t}}\right)\right)\Bigg]\Bigg]. \quad (32)$$

where,

$$\phi(y,t)=\frac{1}{2}\left[e^{-y\sqrt{ScK_c}}erfc\left(\frac{2t\sqrt{K_c}-y\sqrt{Sc}}{2\sqrt{t}}\right)+e^{y\sqrt{ScK_c}}erfc\left(\frac{2t\sqrt{K_c}+y\sqrt{Sc}}{2\sqrt{t}}\right)\right].$$

Letting;

$$b_0 = 1 - MEce^{-\frac{F_1}{Pr}t}\Bigg(1 - erfc\left(\frac{y\sqrt{Pr}}{2\sqrt{t}}\right)\Bigg)\Bigg[GrGce^{-2M_1 t}\Bigg[e^{-y\sqrt{S_cK_c}}erfc\left(\frac{2t\sqrt{K_c}-y\sqrt{Sc}}{2\sqrt{t}}\right) + e^{y\sqrt{ScK_c}}erfc\left(\frac{2t\sqrt{K_c}+y\sqrt{S_c}}{2\sqrt{t}}\right)\Bigg]\left(1-2erfc\left(\frac{y}{2\sqrt{t}}\right)+\left(erfc\left(\frac{y}{2\sqrt{t}}\right)\right)^2\right) + Gr\left(e^{-M_1 t}-e^{-M_1 t}erfc\left(\frac{y}{2\sqrt{t}}\right)\right)\left(-e^{at-y\sqrt{a+M_1}}erfc\left(\frac{2t\sqrt{a+M_1}-y}{2\sqrt{t}}\right) + e^{at+y\sqrt{a+M_1}}erfc\left(\frac{2t\sqrt{a+M_1}+y}{2\sqrt{t}}\right)\right)\Bigg].$$

Equation (32) represents the general solution of the temperature profile for $t>0$. However, there are other possible solutions if $\theta^2(y,t)\neq 0$ but the presence of the discriminant, b^2-4ac in the solution of the resulting quadratic equation makes $\theta(y,t)$ not defined for high parameter values.

With known temperature field, the Nusselt number which is proportional to the rate of heat transfer can be analysed. The effects of $t,\ M,F,H,Ec$ and Pr on the rate of heat transfer will be discussed. In dimensionless form, the Nusselt number is given by;

$$N_u=-\frac{\partial\theta}{\partial y}\Big|_{y=0}=b_0^{-2}\left[\frac{M_1E_c}{2\sqrt{\pi^3t^7}}Gc\ \ e^{-2M_1t-\frac{F_1t}{Pr}}\left(\sqrt{\pi t}(8M_1t+12)\right)erfc\left(\frac{2t\sqrt{K_c}}{2\sqrt{t}}\right)- \frac{\sqrt{S_c}}{\sqrt{\pi t}}Gc^2\,e^{-4tK_c-2M_1t}+\sqrt{S_cK_c}Gc^2\,e^{-2M_1t}erfc\left(\frac{2t\sqrt{K_c}}{2\sqrt{t}}\right)+\frac{\sqrt{S_c}}{\sqrt{\pi t}}e^{-\frac{2t\sqrt{K_c}+M_1t}{4t}}+ \sqrt{S_cK_c}e^{M_1t}erfc\left(\frac{2t\sqrt{K_c}}{2\sqrt{t}}\right)\right]. \quad (33)$$

The rate of mass transfer coefficient at the vertical plate described by the Sherwood number can also be analysed. The effects of t, Sc and K_c on Sherwood number will be examined. In dimensionless form, the Sherwood number is given by;

$$sh=-\left(\frac{\partial\emptyset}{\partial y}\right)_{y=0}=-\frac{\sqrt{S_c}}{\sqrt{\pi t}}e^{-4tK_c}+\sqrt{ScK_c}\left(\frac{2t\sqrt{K_c}}{2\sqrt{t}}\right). \quad (34)$$

Finally, it is significant to analysed the effects on the skin friction due to changes in the physical parameters t,F,H,M,Pr,K_c and k. In dimensionless form, the skin friction is given by;

$$\tau=-\frac{\partial u}{\partial y}\Big|_{y=0}=-\frac{1}{\sqrt{\pi t}}e^{\frac{-M_1}{4}}erfc\left(\frac{2t\sqrt{\frac{F_1}{Pr}}}{2\sqrt{t}}\right)+\frac{1}{\sqrt{\pi t}}e^{\frac{-M_1}{4}}erfc\left(\frac{2t\sqrt{K_c}}{2\sqrt{t}}\right)+\ \frac{1}{\sqrt{\pi t}}e^{\frac{-M_1t}{4t^2}}\big(Gr\theta(y,t)+ G_c\phi(y,t)\big). \quad (35)$$

Results and Discussion

The effects of the physical controlling parameters on the Temperature (θ), Concentration(ϕ) and Velocity (u) profiles were obtained using MATLAB codes and displayed graphically for various conditions of the flow. These results are illustrated and discussed in sub-sections A, B and C.

A. Temperature Profiles

Fig. 2 depicts the influence of Prandtl number (Pr) on the temperature distribution in the flow. It is observed that Pr has the effects of increasing the temperature profile of the fluid as a result of increased fluid viscosity. In Fig. 3., the effects of heat absorption parameter (H) on the temperature profile is depicted. It was observed that the heat absorption parameter increases the temperature of the fluid at away location from the surface since the internal heat of the fluid is retained as the fluid absorbs the atmospheric temperature. Similar observation was made for the radiation parameter in Fig. 4.

The effects of the magnetic parameter (M) and Eckert number (Ec) on the temperature profiles are depicted in Figs. 5 and 6. It is instructive to not that the presence of the magnetic parameter creates an induced force known as the Lorenz force which act to retard the flow and hence the temperature.

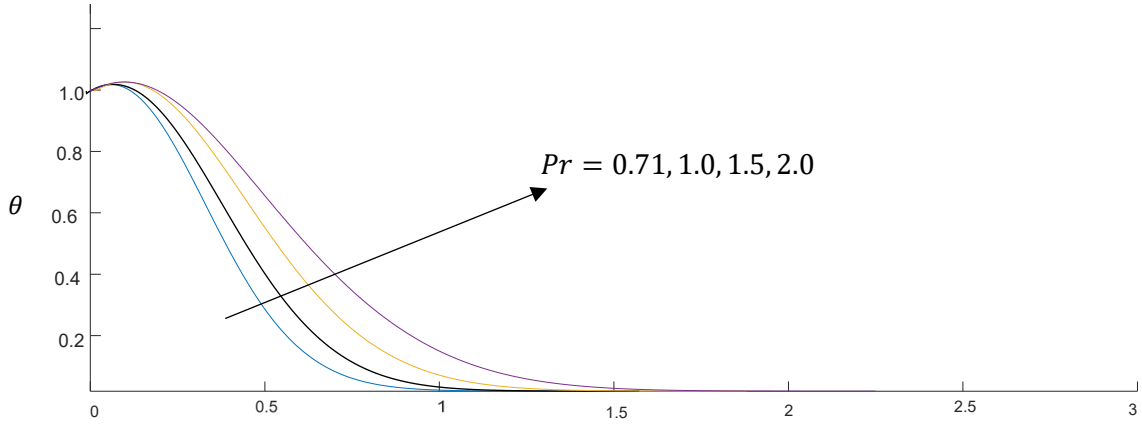

Fig. 2: Effects of **Pr** on the temperature profiles when $\mathbf{Gr = 5, Gc = 5}$, $\mathrm{t = 0.2, k = 1, K_c = 1, S_c = 2.01, a = 0.2, Ec = 1, M = 2, F = 2}$ and $\mathrm{H = 2}$.

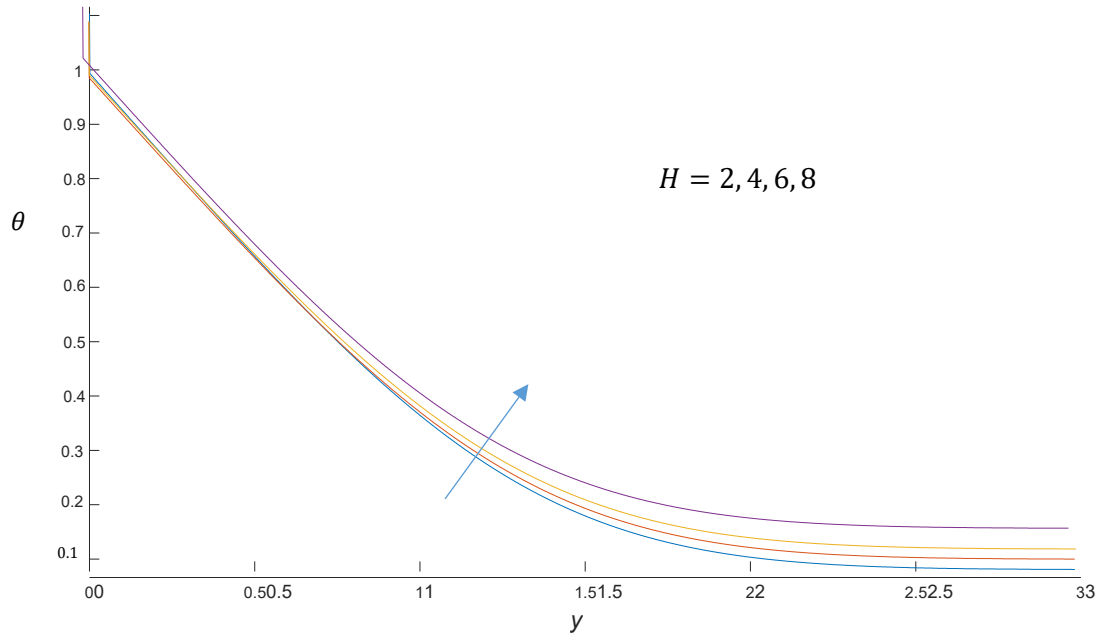

Fig. 3: Effects of **H** on the temperature profiles when $\mathbf{Gr = 5, Gc = 5}$, $\mathrm{t = 0.2, k = 1, K_c = 1, S_c = 2.01, a = 0.2, Ec = 1, M = 2, F = 2}$ and $\mathrm{Pr = 0.71}$.

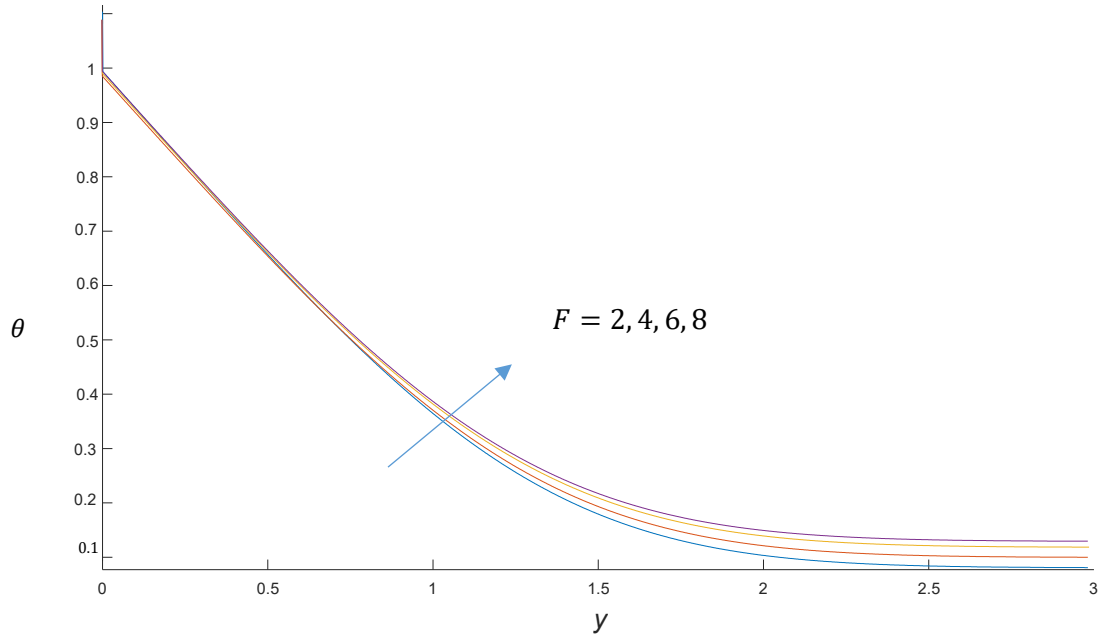

Fig. 4: Effects of $\boldsymbol{F}$ on the temperature profiles when Gr= $\mathbf{5}, \boldsymbol{Gc} = \mathbf{5}$, $t = 0.2, k = 1, K_c = 1, Sc = 2.01, a = 0.2, Ec = 1, M = 2, Pr = 0.71$ and $H = 2$.

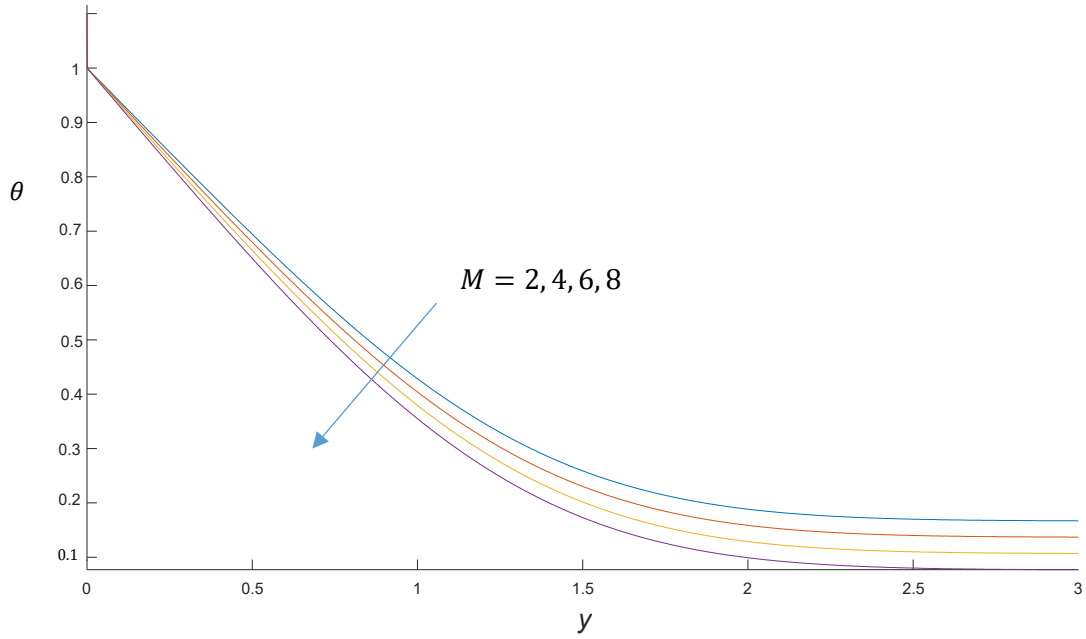

Fig. 5: Effects of $\boldsymbol{M}$on the temperature profiles when $\boldsymbol{Gr} = \mathbf{5}, \boldsymbol{Gc} = \mathbf{5}$, $t = 0.2, k = 1, K_c = 1, Sc = 2.01, a = 0.2, Ec = 1, Pr = 0.71, F = 2$ and $H = 2$.

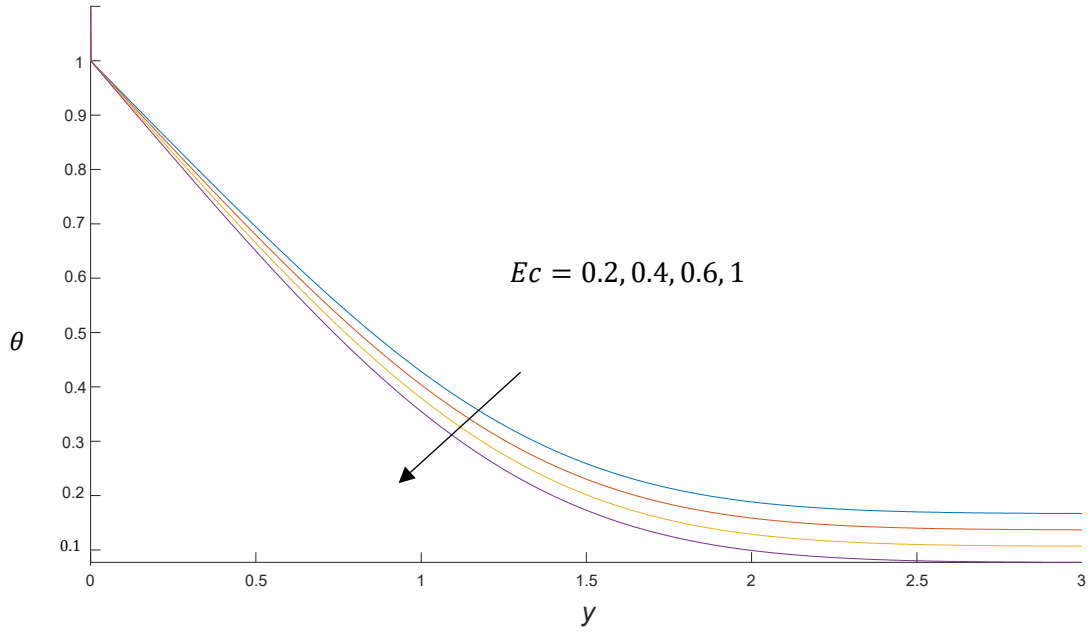

Fig. 6: Effects of $\boldsymbol{Ec}$ on the temperature profiles when $\boldsymbol{Gr = 5, Gc = 5,\ t = 0.2, k = 1, K_c = 1, Sc = 2.01, a = 0.2, Pr = 0.71, M = 2, F = 2}$ and $\boldsymbol{H = 2}$.

B. Concentration Profiles

The main factors that affect the concentration of chemical species in the flow are the reaction rate parameter and the Schmidt number. These are depicted graphically in Figs 7 and 8.

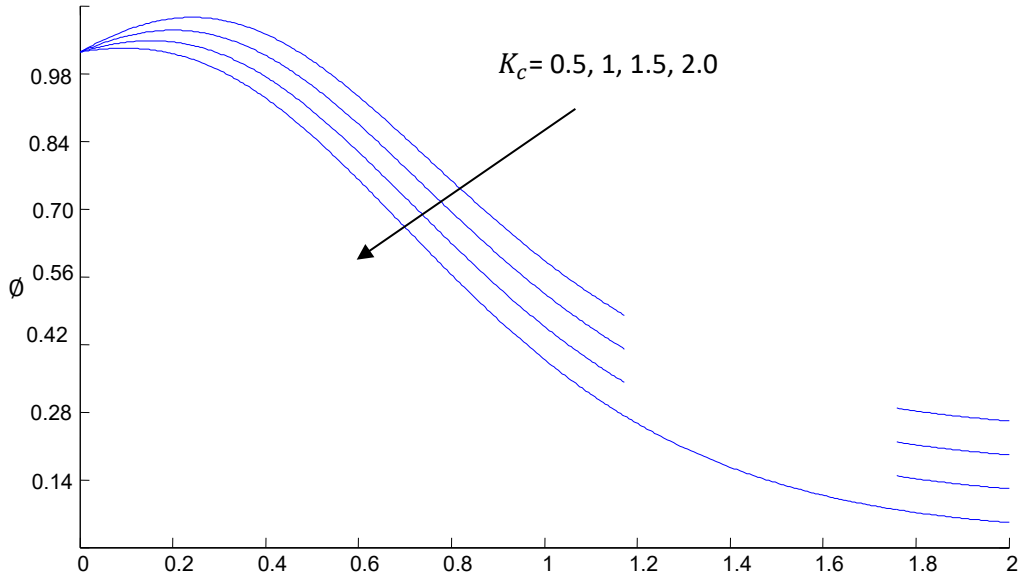

Fig.7: Effects of $\boldsymbol{K_c}$ parameter on the concentration profiles when $\boldsymbol{t = 0.2}$ and $\boldsymbol{Sc = 2.01}$.

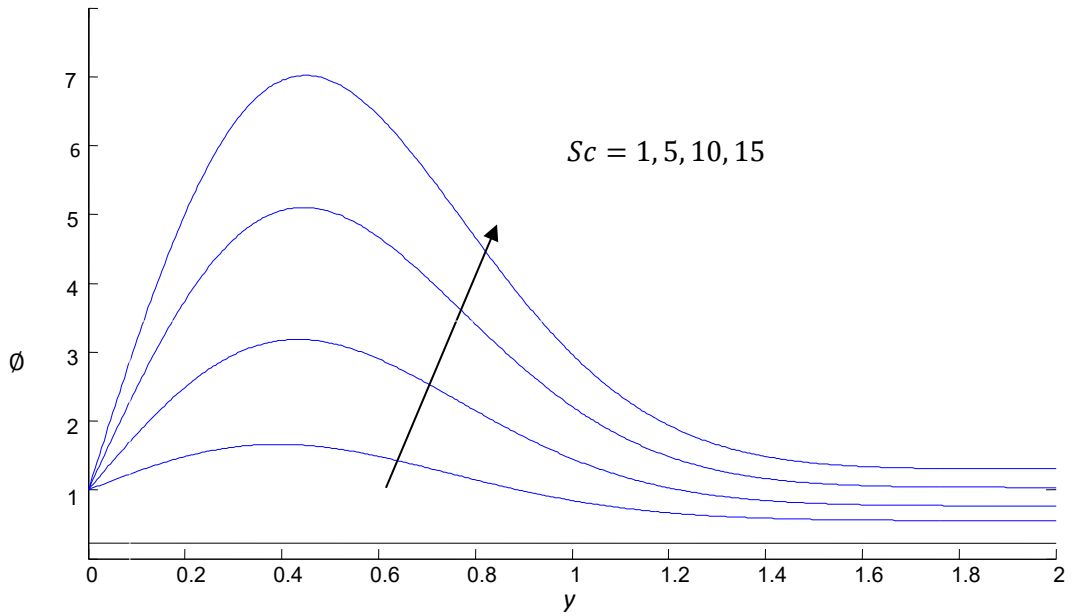

Fig. 8: Effects of Sc on the concentration profiles when $K_c = 1$ and $t = 0.2$.

Figs. 7 and 8 depict the effects of chemical reaction parameter (K_c) and Schmidt number (Sc) respectively on the concentration profiles. It is observed that increasing the chemical reaction parameter, K_c decreases the concentration boundary layer due to the fact that the chemical reaction is destructive leading to a reduced species concentration in fluid. It is also observed in Fig 8 that that the concentration of chemical species increases at all points of the flow particularly close to the surface with increasing values of the Schmidt number.

C. Velocity Profiles

Velocity profiles are illustrated in Figs. 9 – 14 for controlling parameters of $K_c, Sc, Gc,\ Pr,\ M$ and Gr respectively. It is observed that increasing values of K_c, M and Gc retards the motion of the fluid whereas increases in Gr, Pr and Sc hastens the flow.

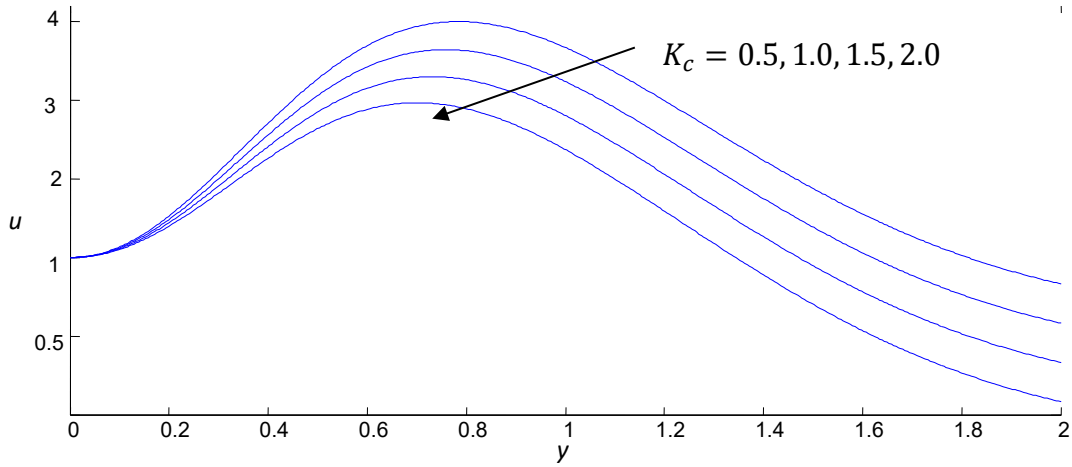

Fig. 9: Effects of $\boldsymbol{K_c}$ on the velocity profiles when $\boldsymbol{Gr = 5, Gc = 5, Ec = 1}$ $t = 0.2, k = 1, Sc = 2.01,\ a = 0.2, Pr = 0.71, M = 2, F = 2$ and $H = 2$.

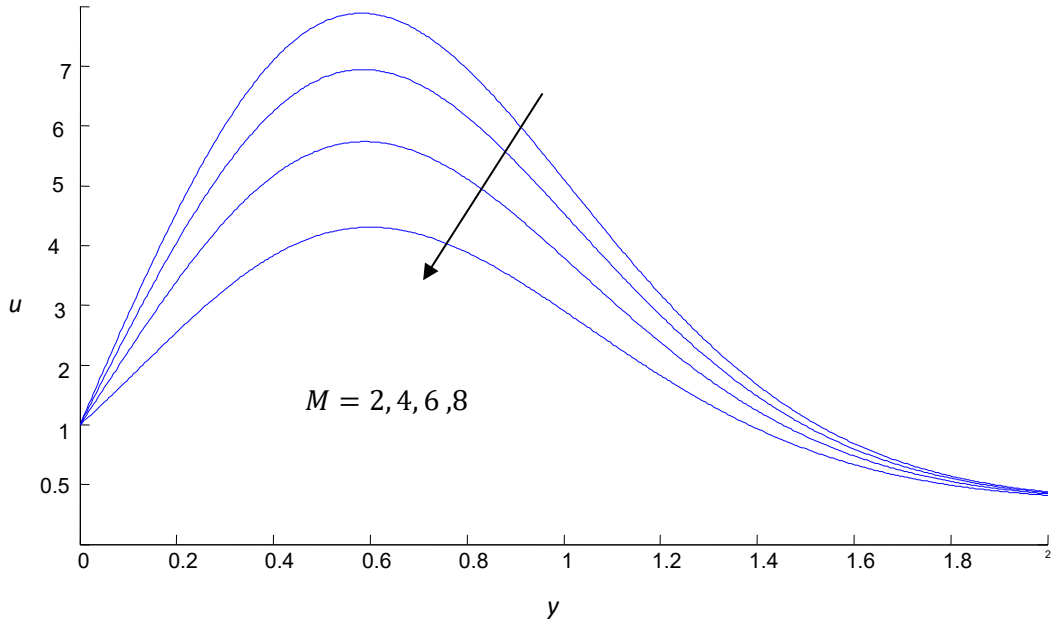

Fig. 10: Effects of $\boldsymbol{M}$on the velocity profiles when $\boldsymbol{Gr = 5}, \boldsymbol{Gc = 5}$, $t = 0.2, k = 1, K_c = 1, Sc = 2.01, a = 0.2, Pr = 0.71, Ec = 2, F = 2$ and $H = 2$.

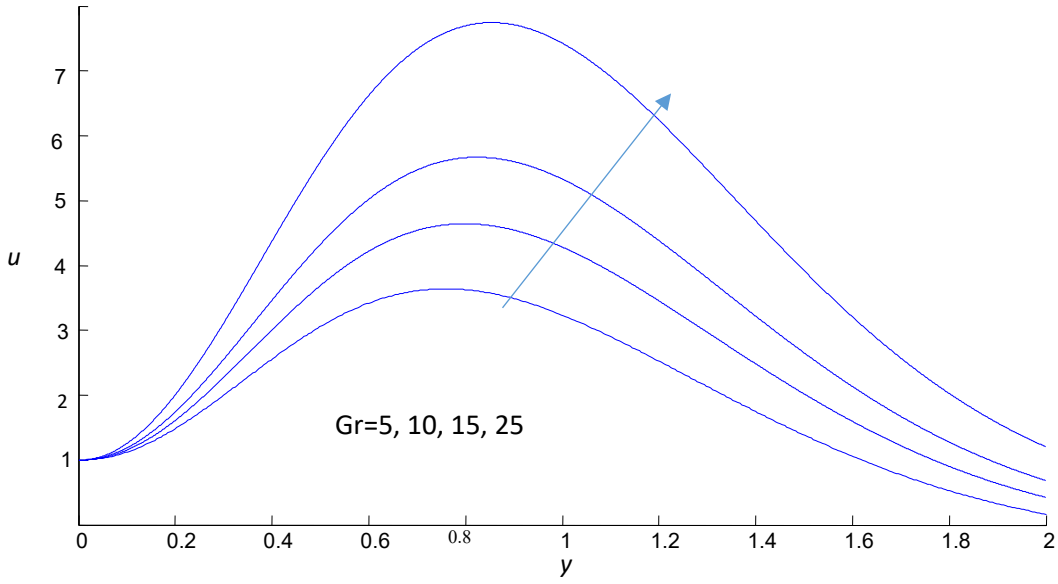

Fig. 11: Effects of $\boldsymbol{G_r}$on the velocity profiles when $\boldsymbol{M = 2}, \boldsymbol{Gc = 5}$, $t = 0.2, k = 1, K_c = 1, Sc = 2.01, a = 0.2, Pr = 0.71, Ec = 2, F = 2$ and $H = 2$.

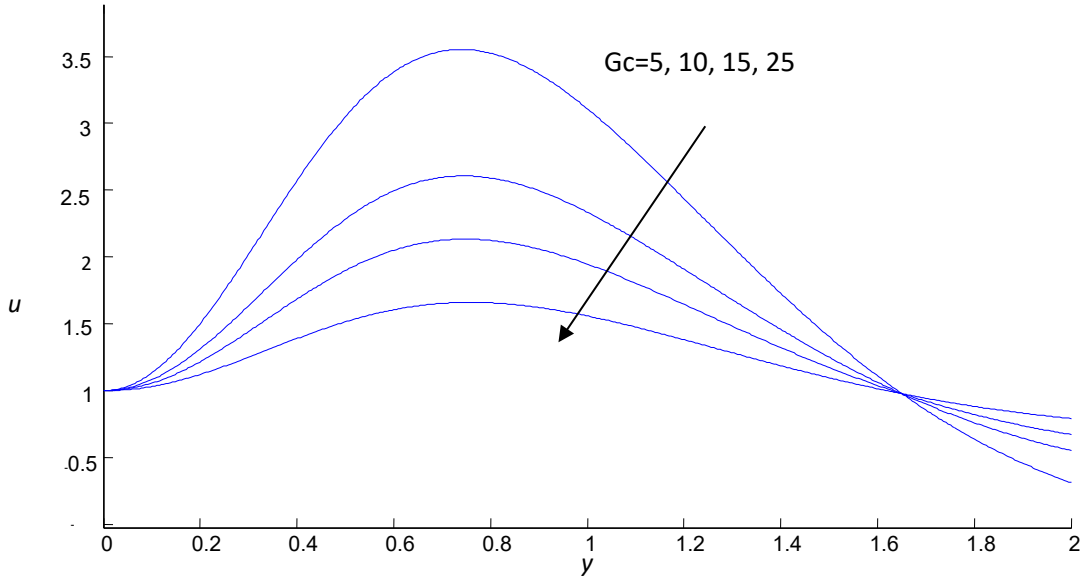

Fig. 12: Effects of Gc on the velocity profiles when $\boldsymbol{M = 2, Gr = 5}$, $t = 0.2, k = 1, K_c = 1, Sc = 2.01, a = 0.2, Pr = 0.71, Ec = 2, F = 2$ and $H = 2$.

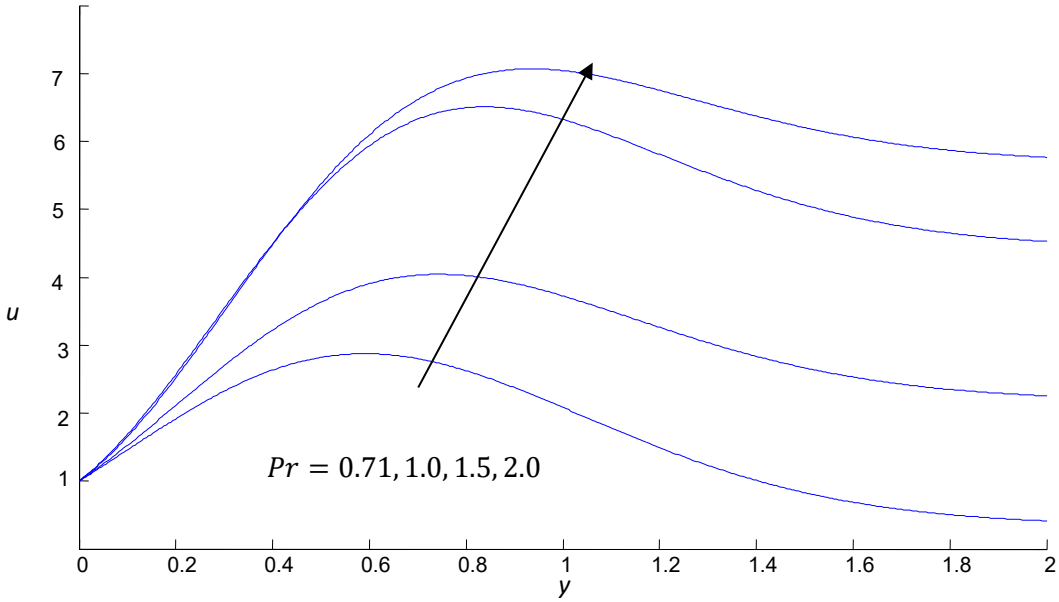

Fig. 13: Effects of Pr on the velocity profiles when $\boldsymbol{M = 2, Gr = 5}$, $t = 0.2, k = 1, K_c = 1, Sc = 2.01, a = 0.2, Gc = 5, Ec = 2, F = 2$ and $H = 2$.

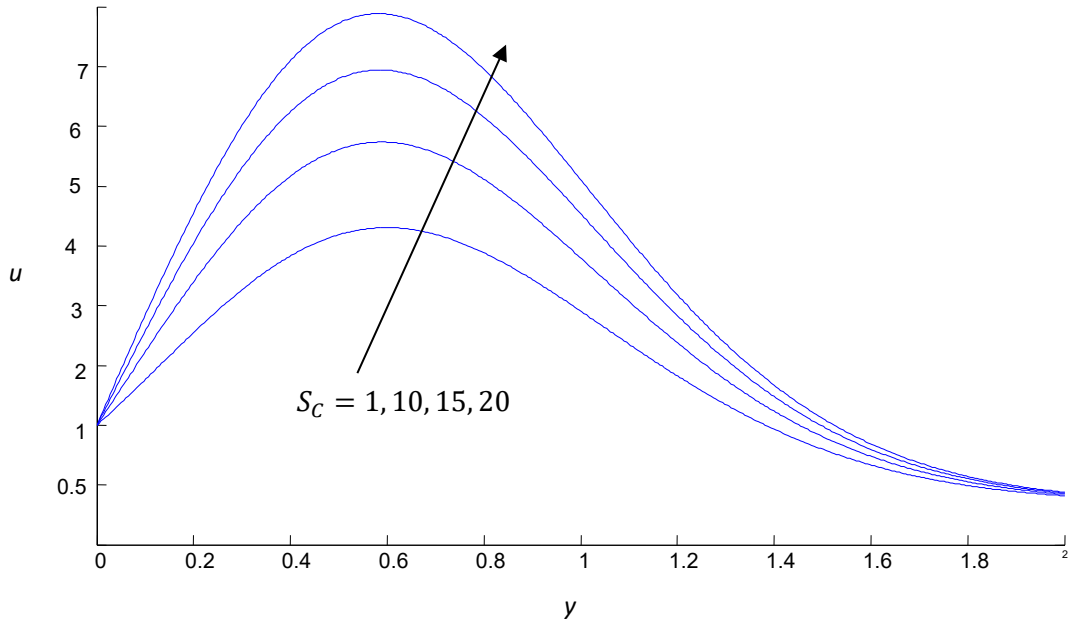

Fig. 14: Effects of $\boldsymbol{Sc}$ on the velocity profiles when $\boldsymbol{M = 2, Gr = 5}$, $t = 0.2, k = 1, K_c = 1, Pr = 0.71, a = 0.2, Gc = 5, Ec = 2, F = 2$ and $H = 2$.

D. Nusselt Number

Figs. 15 - 19 show the effects of Prandtl number (Pr), Magnetic parameter (M), Eckert number (Ec), Radiation parameter (F) and Heat absorption parameter (H) on Nusselt number respectively. It is observed that increases in M or Ec causes a reduction in the Nusselt number which is proportional to the rate of heat transfer from the surface whilst increasing Pr, F and H results in increased rate of heat transfer.

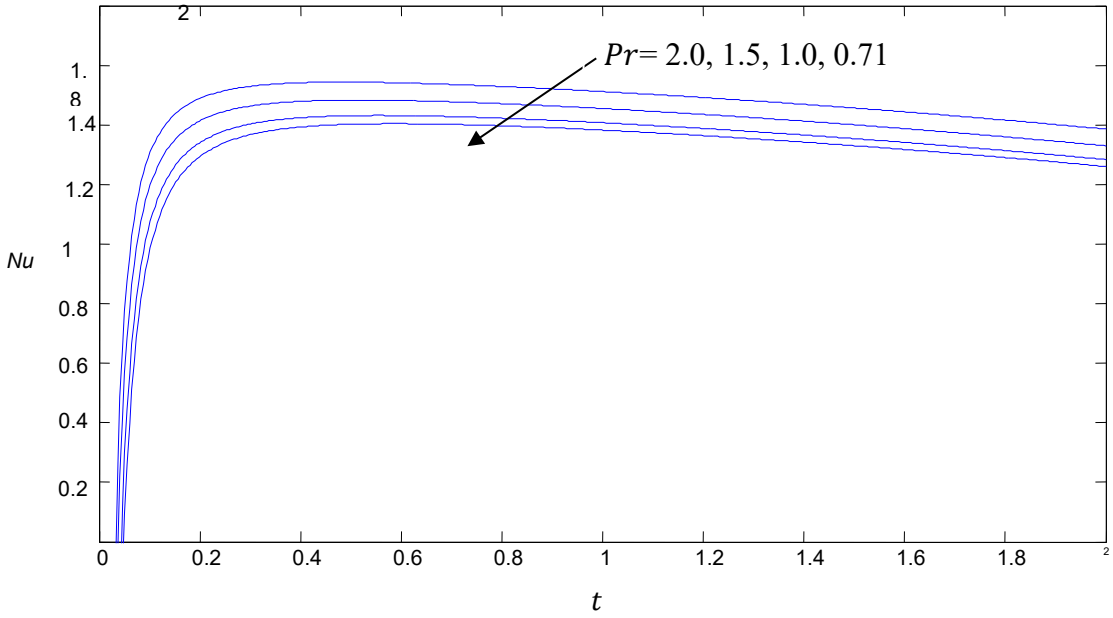

Fig. 15: The effects of $\boldsymbol{Pr}$ on the Nusselt number profiles when $\boldsymbol{M = 2}$, $t = 0.2, k = 1, K_c = 1,\ Gr = 5, Gc = 5, Ec = 2, F = 2$ and $H = 2$.

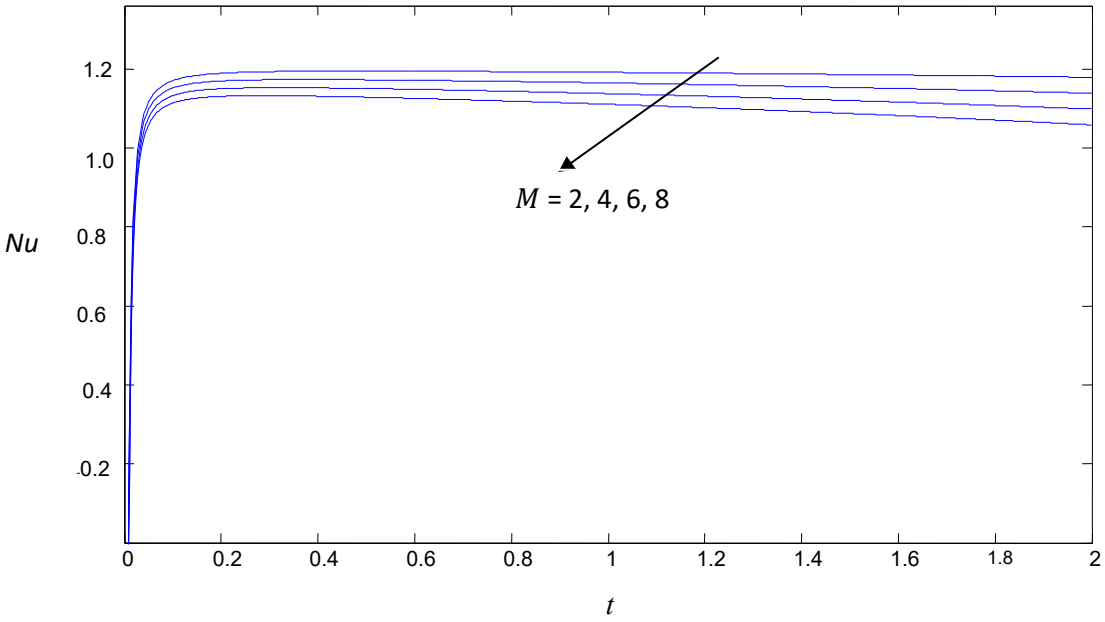

Fig. 16: The effects of M on the Nusselt number profiles when $\boldsymbol{Pr = 0.71}$, $t = 0.2, k = 1, K_c = 1,\ Gc = 5, Gr = 5, Ec = 1, F = 2$ and $H = 2$.

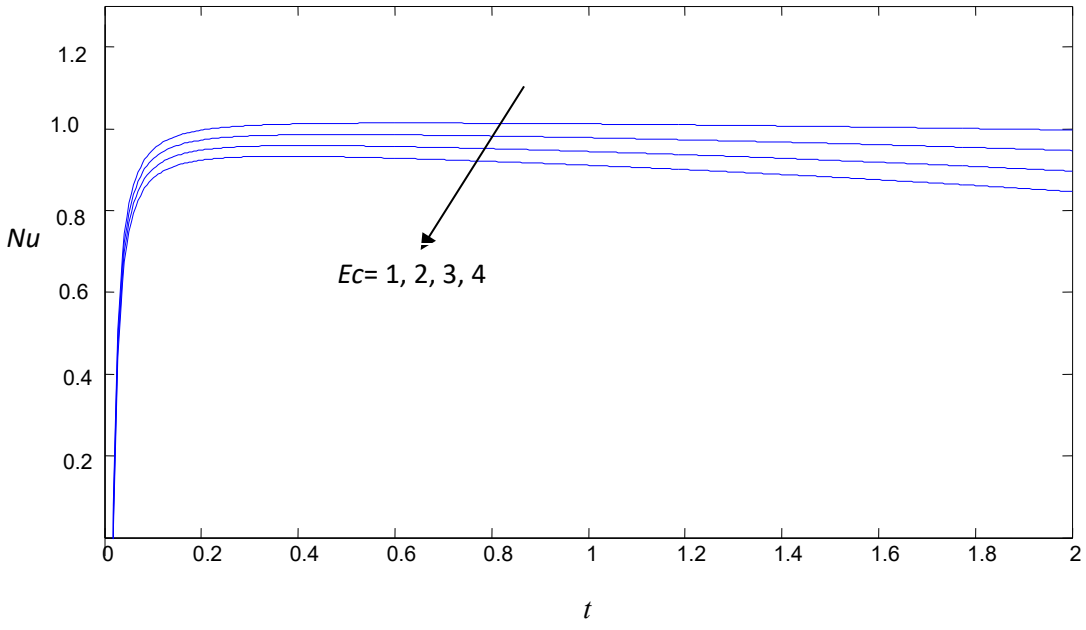

Fig. 17: The effects of Ec on the Nusselt number profiles when $\boldsymbol{Pr = 0.71}$, $t = 0.2, k = 1, K_c = 1,\ Gr = 5,\ Gc = 5, M = 2, F = 2$ and $H = 2$.

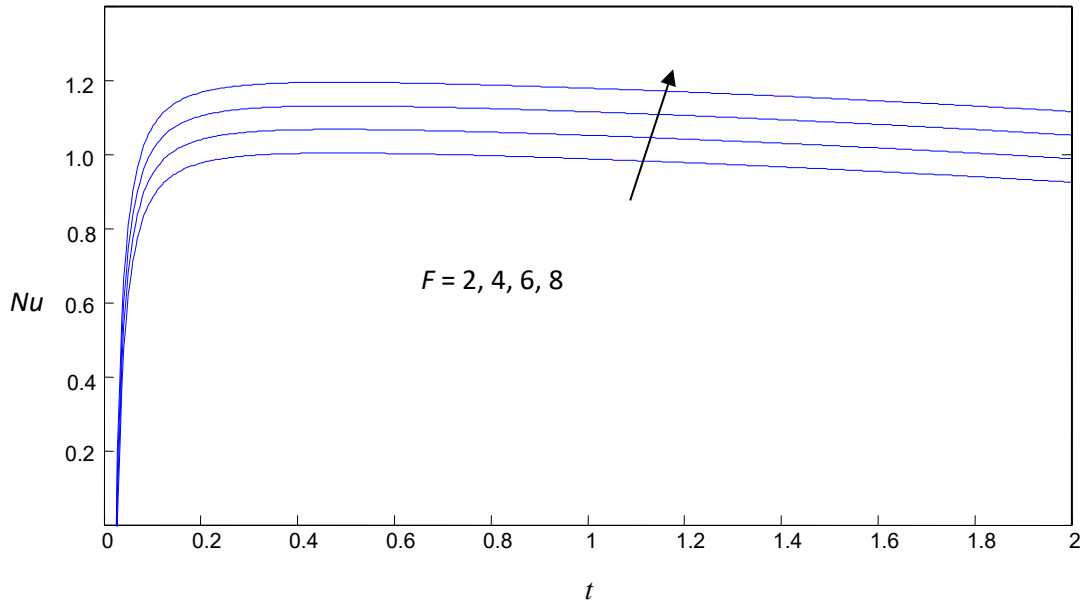

Fig. 18: The effects of F on the Nusselt number profiles when $\boldsymbol{Ec = 0.71}$, $t = 0.2, k = 1, K_c = 1,\ Gc = 5,\ Gr = 5, Ec = 2, F = 2$ and $H = 2$.

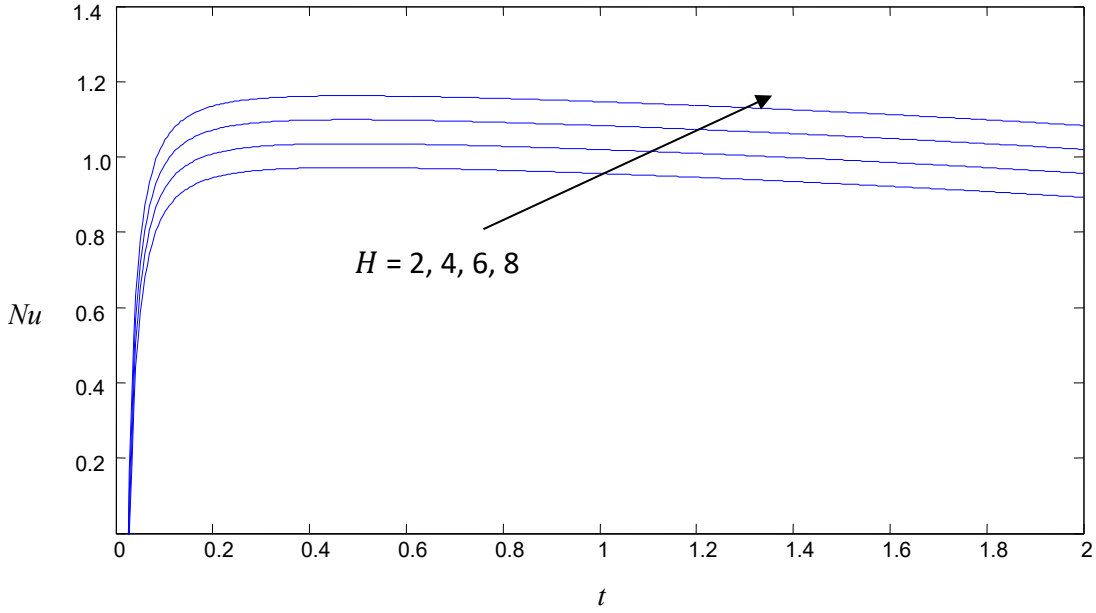

Fig. 19: The effects of $\boldsymbol{H}$ on the Nusselt number profiles when $\boldsymbol{Pr = 0.71}$, $t = 0.2, k = 1, K_c = 1,\ Gc = 5, Gr = 5, Ec = 1, F = 2$ and $M = 2$.

E. Sherwood Number Profiles

Figs. 20 and 21 illustrate the effects of Schmidt number (*Sc*) and Chemical reaction parameter (*Kc*) on the Sherwood number respectively. It is observed that an increase in *Sc* increases the Sherwood Number which is proportional to the rate of mass transfer whilst increasing *Kc* reduces the rate of mass transfer for obvious reasons.

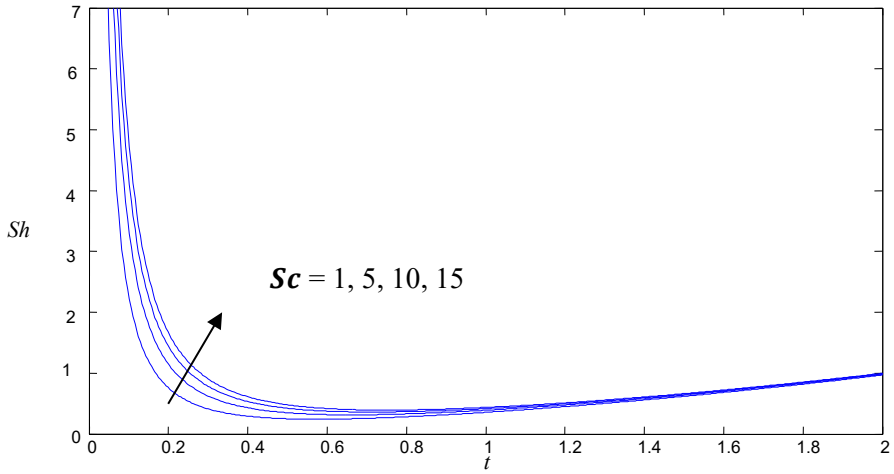

Fig. 20: Effects of on the Sherwood number profiles when $t = 0.2$ and $K_c = 1$.

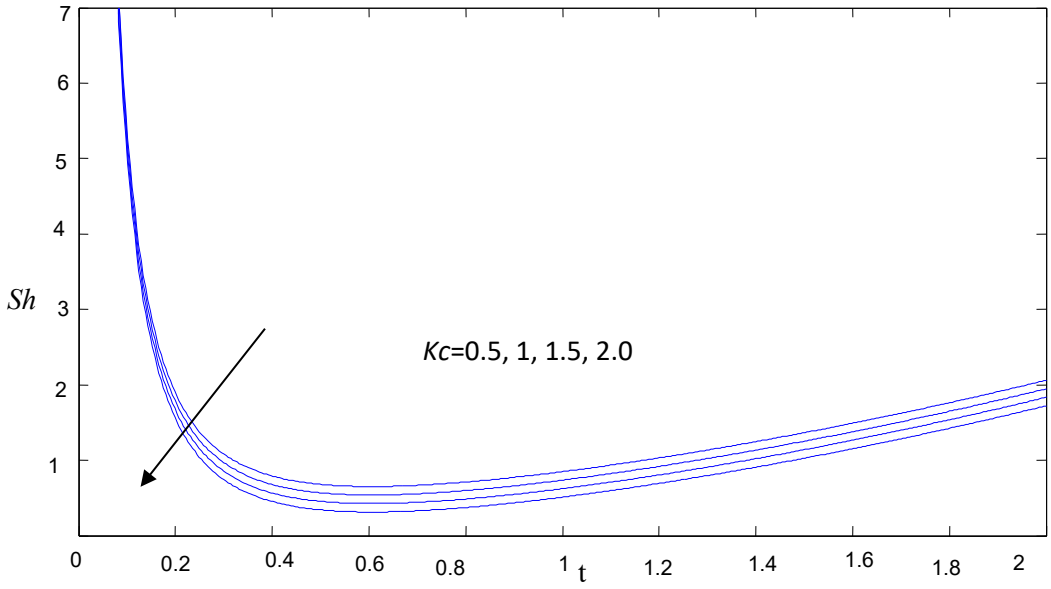

Fig. 21: Effects of *Kc* on the Sherwood number profiles when $\boldsymbol{t = 0.2}$ **and** $\boldsymbol{Sc = 2.01}$.

F. Skin Friction Profiles

Figs. 22 and 23 depicts the effects of permeability of the porous medium (k) and magnetic parameter (M) on the skin friction coefficient respectively. It is noticed that an increase in M results in decrease in the Skin Friction coefficient whilst increase in k results in increase in the Skin Friction coefficient

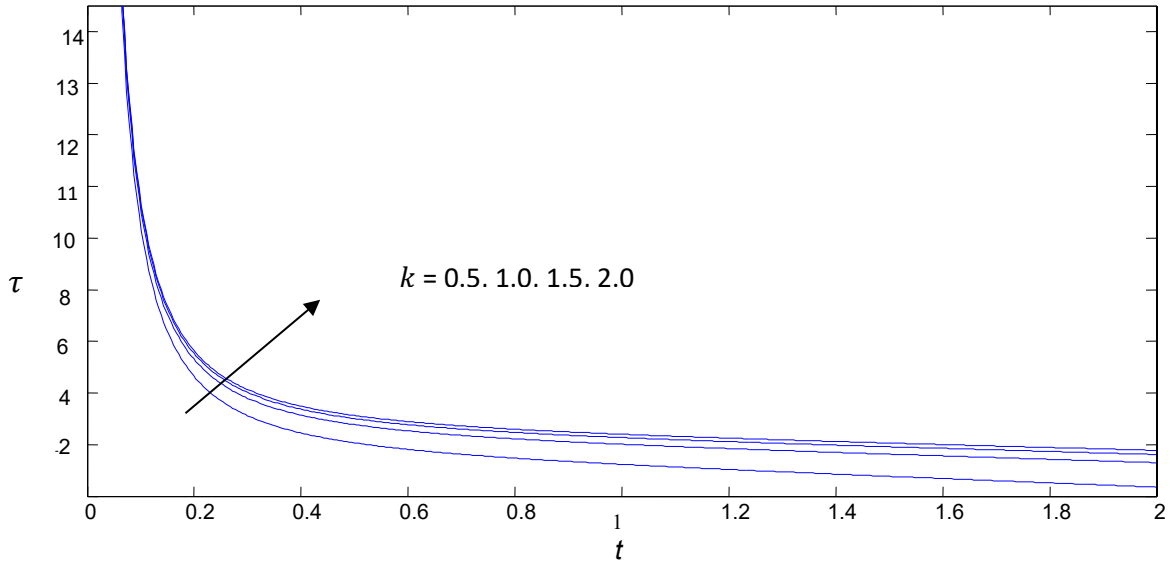

Fig. 22: Effects of k on the Skin Friction coefficient when $t = 0.2,\ K_c = 1, H = 2,\ F = 2, Pr = 0.71$ and $M = 2$.

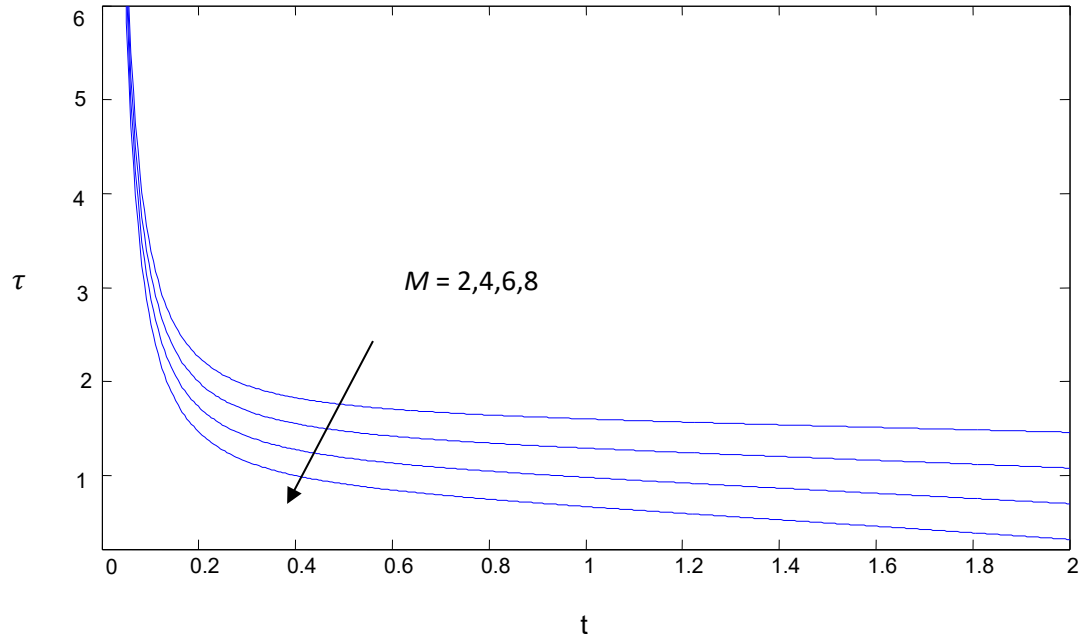

Fig. 23: Effects of Mon the Skin Friction coefficient profiles when $t = 0.2,\ K_c = 1, H = 2,\ F = 2, P_r = 0.71$ and $k = 1$.

Numerical Results

Table 1 – 3 depict the numerical results for the skin friction coefficient,$-u'(0)$, the Sherwood number, $-\emptyset'(0)$ and the Nusselt number, $-\theta'(0)$ for varying parameter values of the controlling parameters. In Table 1, it is noted that the skin friction coefficient, $-u'(0)$ decreases for increasing values of t, M, Pr and K_c but increases with increasing values of k, F and H.

The skin friction co-efficient reduces with time as the layer of fluid flows on each other serving as lubricants. The magnetic field parameter introduces the Lorenz force which acts to oppose the motion. However, the absorption and radiation parameters as well as the reaction parameter increase the molecular activity within the flow leading to increase internal energy, thereby increasing the skin friction on the surface.

Table 1: The Skin friction coefficient, -u' (0) at the wall for varying values of t, M, k, F, H, Pr and K_c.

t	M	k	F	H	Pr	K_c	$-u'(0)$
0.2	1.0	1.0	1.0	1.0	1.0	1.0	0.1194
0.4	1.0	1.0	1.0	1.0	1.0	1.0	0.0894
0.6	1.0	1.0	1.0	1.0	1.0	1.0	0.0671
0.2	1.5	1.0	1.0	1.0	1.0	1.0	0.1053
0.2	2.0	1.0	1.0	1.0	1.0	1.0	0.0930
0.2	2.5	1.0	1.0	1.0	1.0	1.0	0.0820
0.2	1.0	2	1.0	1.0	1.0	1.0	0.1353
0.2	1.0	4	1.0	1.0	1.0	1.0	0.1440
0.2	1.0	6	1.0	1.0	1.0	1.0	0.1469
0.2	1.0	1.0	2	1.0	1.0	1.0	0.1942
0.2	1.0	1.0	2.5	1.0	1.0	1.0	0.2222
0.2	1.0	1.0	3	1.0	1.0	1.0	0.2458
0.2	1.0	1.0	1.0	2	1.0	1.0	0.1942
0.2	1.0	1.0	1.0	2.5	1.0	1.0	0.2222
0.2	1.0	1.0	1.0	3	1.0	1.0	0.2458
0.2	1.0	1.0	1.0	1.0	0.71	1.0	0.1826
0.2	1.0	1.0	1.0	1.0	1.0	1.0	0.1194
0.2	1.0	1.0	1.0	1.0	1.5	1.0	0.0473
0.2	1.0	1.0	1.0	1.0	1.0	0.4	0.2434
0.2	1.0	1.0	1.0	1.0	1.0	0.6	0.1937

Table 2 depicts the numerical results for the Sherwood number, $-\emptyset'(0)$ for varying controlling parameter values of t Sc and K_c. It revealed that the rate of mass transfer decreases with increasing time and chemical reaction parameter but increases with increasing Schmidt number. At low *Sc*, particles exhibit greater diffusivity and are very small to be conditioned by the viscosity of the medium. At high *Sc*, particles are giant with small diffusivity and the deposition becomes less and less relevant.

The reaction rate parameter essentially indicates the effectiveness of the chemical reaction. It is directly affected by the rate of mixing. A higher reaction rate parameter means that molecules are mixing at a faster rate thereby decreasing the rate of mass transfer as a result of the destructive chemical reaction.

Table 2: Sherwood number -$\emptyset'(0)$ for various values of $\boldsymbol{time}\ (\boldsymbol{t}), \boldsymbol{Schmidt\ number}\ (\boldsymbol{Sc})\ \boldsymbol{and}$ and reaction rate parameter ($\boldsymbol{K_c}$).

t	S_c	K_c	$-\emptyset'(0)$
0.2	1.0	1.0	1.0141
0.4	1.0	1.0	0.8126
0.6	1.0	1.0	0.8047
0.2	0.2	1.0	0.4535
0.2	0.4	1.0	0.6414
0.2	0.6	1.0	0.7855
0.2	1.0	0.2	1.1645
0.2	1.0	0.4	1.0950
0.2	1.0	0.6	1.0490

In Table 3, numerical results for the Nusselt number $-\theta'(0)$ is presented. It is observed that the rate of heat transfer decreases with time magnetic parameter and Eckert number. The magnetic parameter causes and induced force to act opposing the flow thereby reducing the rate of heat transfer at the surface. Conversely, $Pr, F, Gc, K_c$and Sc contributes to the rate of heat transfer.

Table 3: The local Nusselt number, -θ' (0) for varying values of $\boldsymbol{t, M, Ec, Gc, F, Pr, K_c}$, Sc when $\boldsymbol{k = 1}$ and $\boldsymbol{H = 1}$.

t	M	Ec	Gc	F	Pr	K_c	Sc	$-\theta'(0)$
0.2	1	1	1	1	1	1	1	1.7623
0.4	1	1	1	1	1	1	1	0.6154
0.6	1	1	1	1	1	1	1	0.2877
0.2	2	1	1	1	1	1	1	0.6075
0.2	4	1	1	1	1	1	1	0.0482
0.2	6	1	1	1	1	1	1	0.0037
0.2	1	0.2	1	1	1	1	1	1.0574
0.2	1	0.4	1	1	1	1	1	0.7049
0.2	1	0.6	1	1	1	1	1	0.3525
0.2	1	1	5	1	1	1	1	0.6611
0.2	1	1	7	1	1	1	1	0.6943
0.2	1	1	9	1	1	1	1	1.3111
0.2	1	1	1	2	1	1	1	0.0005
0.2	1	1	1	4	1	1	1	0.0056

0.2	1	1	1	6	1	1	1	0.6075
0.2	1	1	1	1	0.7	1	1	0.0898
0.2	1	1	1	1	1.0	1	1	0.6075
0.2	1	1	1	1	1.2	1	1	0.3251
0.2	1	1	1	1	1	0.2	1	0.0458
0.2	1	1	1	1	1	0.4	1	0.1192
0.2	1	1	1	1	1	0.6	1	0.2338
0.2	1	1	1	1	1	1	2	0.3372
0.2	1	1	1	1	1	1	3	0.4107
0.2	1	1	1	1	1	1	4	0.4778

Conclusion

The time-dependent hydrodynamic boundary layer flow in the presence of internal heat generation in porous media has been investigated. The non-linear partial differential equations have been modelled and transformed using similarity variables. The Laplace transform techniques has been employed to solve the resulting dimensionless differential equations exactly and results illustrated graphically and numerically in tables. From the results obtained, the following conclusions can be drawn:

i. The thermal boundary layer thickness can be controlled with the application of a transverse magnetic field. The boundary layer can however be enhanced with viscous fluids and the heat absorption (H) or radiation (F) parameters.

ii. The solutal boundary layer thickness increases with the Schmidt number (Sc) whilst the chemical reaction parameter (K_c) causes a reduction in the species concentration in the fluid.

iii. The speed of flow is reduced with increasing chemical reaction parameter (K_c), magnetic field parameter (M) and solutal Grashof number (Gc) but increases with increasing thermal Grashof number (Gr) and the Schmidt number (Sc).

iv. The Nusselt number is decreased with higher values of the magnetic parameter (M) and Eckert number (Ec) but increases with higher values of the Prandtl number (Pr), the radiation parameter (F) and the heat absorption parameter (H).

v. The rate of mass transfer in the fluid is decreased with time (t) and chemical reaction parameter (K_c) but increases with the Schmidt number (Sc).

vi. The skin friction coefficient decreases with increasing time (t), magnetic field parameter (M), Prandtl number (Pr), and chemical reaction parameter (K_c) but increased with increasing permeability of porous medium (k), radiation parameter (F) and heat absorption parameter (H).

References

[1] R.C. Chaudhary and P. Jain, Unsteady free convection boundary layer flow past an impulsively started vertical surface with Newtonian heating, Rom. J. Phys., 51 (9-10), (2006), 911-925.

[2] A.S. Gupta, I. Pop, and V.G. Soundalgekar, Free convection flow past a linearly accelerated vertical plate on the presence of viscous dissipation heat, Rev. Roum. Sci. Techn. Mec Apl. 24 (1979) 561-568.

[3] N.G. Kafousias, and A.A. Raptis, Mass transfer effects subject to variable suction or injection, *Rev. Roum. Sci. Techn. Mec. Apl. 26,* (1981) *11-22.*

[4] D. Lesnic, D. B. Ingham and I. Pop, Free convection boundary layer flow along a vertical surface in a porous medium with Newtonian heating, Int. J. Heat Mass Transfer, 42, (1999). 2621-2627.

[5] F. Constantin, I. K. Samiulhaq, A. Fard and S. Sharidan, Radiation and Porosity Effects on the Magnetohydrodynamic Flow Past an Oscillating Vertical Plate with Uniform Heat Flux, Z. Naturforsch. 67a, 572 – 580 (2012) / DOI: 10.5560/ZNA.2012-0070.

[6] R. Muthucumaraswamy and S. Janakiraman, Mass transfer effects on exponentially accelerated isothermal vertical plate. *Theoret. Aple. Mech. 33(1),* (2006) *17-29.*

[7] P.A.R. Bala, N.R. Bhaskar, and S. Suneetha, Effects on MHD flow past an exponentially accelerated isothermal vertical plate embedded in porous medium in the presence of heat source and chemical reaction, J. Applied Fluid Mechanics, 5(3) (2012) 119-126.

[8] B.R. Rout and H.B. Pattanayak, Chemical reaction and radiation effect on MHD flow past an exponentially accelerated vertical plate in the presence of heat source with variable temperature embedded in a porous medium, Mathematical theory and Modeling 3(8), (2013) 18-25

[9] Y.I. Seini, Flow over unsteady stretching surface with chemical reaction and non-uniform heat source. J. Eng. Manu. Technol. 1 (2013) 24-35

[10] Y.I. Seini and O.D. Makinde (2013). MHD Boundary Layer Flow due to Exponential Stretching Surface with Radiation and Chemical Reaction, Mathematical Problems in Engineering, (2013) 1- 7.

[11] I.Y. Seini, G. Aloliga, B. Ziblim, O.D. Makinde, Boundary Layer Flow of Casson Fluid on Exponentially Stretching Porous Surface with Radiative Heat Transfer. Diffusion Foundations 26, (2020) 112-125

[12] C.J. Etwire, I.Y. Seini, M. Rabiu, O.D. Makinde, Impact of thermophoretic transport of Al_2O_3 nanoparticles on viscoelastic flow of oil-based nanofluid over a porous exponentially stretching surface with activation energy. Engineering Transactions 67(3) (2019) 387–410

[13] I.Y. Seini, Heat and mass transfer from a convectively heated vertical surface with chemical reaction and internal heat generation . Engineering Transactions 67(1) (2019) 101–118

[14] M. Ali, M.D. Abdul Alim and S.A. Mohammed, Heat transfer boundary layer flow past an inclined stretching sheet in the presence of magnetic field, Int. J. of Advancements in Research & Technology, 3(5) (2014), 34-40.

[15] A.J. Chamkha, M.C. Raju, R.T. Sudhakar and S.V.K. Varma, Unsteady MHD free convection flow past an exponentially accelerated vertical plate with mass transfer, chemical and thermal radiation, Int. J. of Microscale and Nanoscale thermal 5(1) (2016) 57-75.

[16] E.M. Arthur T. Ayando and Y.I. Seini, MHD convective boundary layer flow towards a vertical surface in a porous medium with radiation, chemical reaction and internal heat generation, Frontiers in Heat and Mass Transfer (FHMT),6(21) (2015) 1-10.

[17] A. Hussanan, M.Z. Salleh, I. Khan, and R.M. Tahar, Unsteady boundary layer flow and heat transfer of a Casson fluid past an oscillating vertical plate with Newtonian heating, Plos One,9(10), e108763. (2014).

[18] A. Hussanan, M.Z. Salleh, I. Khan, R.M. Tahar and Z. Ismail, Soret effects on unsteady MHD mixed convective heat and mass transfer flow in a porous medium with Newtonian heating. Maejo Int. J. Sci. and Tech, 9(02) (2015) 224-245.

[19] M. Sulemana, I.Y. Seini and M.I. Daabo, Unsteady boundary layer flow past a vertical plate in the presence of transverse magnetic field and heat source embedded in a porous medium, J. Math and Comp. Sci., 7(3) (2017) 564-582.

[20] M. Sulemana, I.Y. Seini, and M.I. Daabo, Unsteady hydromagnetic convective heat and mass transfer flow past an impulsively started infinite vertical surface with Newtonian heating in a porous medium, J. Eng. and Applied Sci. 12(1) (2017) 5767-5776.